Acta Pharmaceutica Sinica B 2025;15(6):3107−3124

Chinese Pharmaceutical Association
Institute of Materia Medica, Chinese Academy of Medical Sciences

Acta Pharmaceutica Sinica B

www.elsevier.com/locate/apsb
www.sciencedirect.com

ORIGINAL ARTICLE

Ablation of macrophage transcriptional factor FoxO1 protects against ischemia−reperfusion injury-induced acute kidney injury

Yao He[a,†], Xue Yang[a,b,†], Chenyu Zhang[a,†], Min Deng[a,b,†], Bin Tu[c,†], Qian Liu[a], Jiaying Cai[a], Ying Zhang[a,d], Li Su[e], Zhiwen Yang[a,d], Hongfeng Xu[a], Zhongyuan Zheng[a], Qun Ma[a], Xi Wang[a], Xuejun Li[a], Linlin Li[b,*], Long Zhang[d,*], Yongzhuo Huang[f,*], Lu Tie[a,*]

[a]*Department of Pharmacology, School of Basic Medical Sciences, Peking University and Beijing Key Laboratory of Tumor Systems Biology, Peking University, Beijing 100191, China*
[b]*Department of Pharmacology, Xinjiang Medical University, Xinjiang 830011, China*
[c]*Zhongshan Hospital of Traditional Chinese Medicine Affiliated to Guangzhou University of Traditional Chinese Medicine, Zhongshan 528400, China*
[d]*Department of Wound Healing Center and Interventional Radiology and Vascular Surgery, Peking University Third Hospital, Beijing 100191, China*
[e]*Medical and Health Science Analysis Center, Peking University, Beijing 100191, China*
[f]*State Key Laboratory of Drug Research, Shanghai Institute of Materia Medica, Chinese Academy of Sciences, Shanghai 201203, China*

Received 22 July 2024; received in revised form 19 October 2024; accepted 26 November 2024

KEY WORDS

AKI;
I/R injury;
FoxO1;
Macrophage;
Chemotaxis;
Inflammation;

Abstract Acute kidney injury (AKI) has high morbidity and mortality, but effective clinical drugs and management are lacking. Previous studies have suggested that macrophages play a crucial role in the inflammatory response to AKI and may serve as potential therapeutic targets. Emerging evidence has highlighted the importance of forkhead box protein O1 (FoxO1) in mediating macrophage activation and polarization in various diseases, but the specific mechanisms by which FoxO1 regulates macrophages during AKI remain unclear. The present study aimed to investigate the role of FoxO1 in macrophages in the pathogenesis of AKI. We observed a significant upregulation of FoxO1 in kidney macrophages following

*Corresponding authors.
E-mail addresses: tielu@bjmu.edu.cn (Lu Tie), yzhuang@simm.ac.cn (Yongzhuo Huang), longzh2000@163.com (Long Zhang), llltougao@sina.com (Linlin Li).
[†]These authors made equal contributions to this work.
Peer review under the responsibility of Chinese Pharmaceutical Association and Institute of Materia Medica, Chinese Academy of Medical Sciences.

https://doi.org/10.1016/j.apsb.2025.04.009

Migration;
ARHGEF1

ischemia−reperfusion (I/R) injury. Additionally, our findings demonstrated that the administration of FoxO1 inhibitor AS1842856-encapsulated liposome (AS-Lipo), mainly acting on macrophages, effectively mitigated renal injury induced by I/R injury in mice. By generating myeloid-specific FoxO1-knockout mice, we further observed that the deficiency of FoxO1 in myeloid cells protected against I/R injury-induced AKI. Furthermore, our study provided evidence of FoxO1's pivotal role in macrophage chemotaxis, inflammation, and migration. Moreover, the impact of FoxO1 on the regulation of macrophage migration was mediated through RhoA guanine nucleotide exchange factor 1 (ARHGEF1), indicating that ARHGEF1 may serve as a potential intermediary between FoxO1 and the activity of the RhoA pathway. Consequently, our findings propose that FoxO1 plays a crucial role as a mediator and biomarker in the context of AKI. Targeting macrophage FoxO1 pharmacologically could potentially offer a promising therapeutic approach for AKI.

1. Introduction

Acute kidney injury (AKI) is associated with significant morbidity and mortality, thereby increasing the susceptibility to chronic kidney disease and end-stage renal disease[1-3]. Renal ischemia−reperfusion (I/R) injury serves as a common cause of AKI and also occurs in many clinical events, including kidney transplantation, and cardiac and vascular surgery[4,5]. Given the absence of effective clinical drugs and management strategies, an enhanced understanding of the molecular mechanisms underlying AKI would facilitate the development of innovative therapeutic approaches[6,7].

Following renal I/R injury, tubular epithelial cells (TECs) undergo programmed cell death, namely apoptosis and/or necrosis, resulting in the release of pro-inflammatory cytokines and chemokines. These molecules play a crucial role in the recruitment of immune cells, thereby contributing to the pathogenesis of renal injury after I/R injury[5]. Various immune cells from both the innate and adaptive immune systems, including neutrophils, dendritic cells, macrophages, and lymphocytes, actively participate in this process[8]. Notably, a recent study utilizing single-cell RNA sequencing demonstrated a significant infiltration of immune cells, particularly macrophages, in a murine model of renal I/R injury[9]. Furthermore, the presence of macrophage infiltration has been documented in kidney biopsy tissues of individuals with AKI[10]. Macrophages play a significant role in the inflammatory response associated with AKI[11]. Characterized by heterogeneity and plasticity, macrophages polarize into two pro-inflammatory and anti-inflammatory phenotypes regarding the biological and pathological environment[12]. These different phenotypes are important in excessive inflammation and tubular regeneration of acute kidney injury[13,14].

FoxO1, a member of the forkhead transcription factors family, exhibits widespread expression in mammals[15]. FoxO1 plays crucial roles in the regulation of genes involved in various cellular processes such as cell metabolism, proliferation, differentiation, and apoptosis[16,17]. Our previous study has demonstrated that renal I/R injury induces an up-regulation of FoxO1 expression in the kidney. Moreover, the administration of the FoxO1-selective inhibitor AS1842856 could mitigate renal injury induced by I/R injury and improve renal function[18]. Emerging evidence has revealed the significant role of FoxO1 in the activation and polarization of macrophages, which has been extensively investigated in various pathological conditions, including infections, metabolic disorders, fibrosis, and autoimmune diseases[19-22]. Lee and colleagues[20] have specifically identified FoxO1 as a crucial linking overnutrition to hepatic inflammation by regulating macrophage polarization, and myeloid cell conditional FoxO1 knockout skewed macrophage polarization from pro-inflammatory to the anti-inflammatory phenotype. In the tumor microenvironment, FoxO1 facilitated anti-inflammatory macrophage polarization and the recruitment of anti-inflammatory macrophages in the tumor microenvironment[23]. Nevertheless, the role of FoxO1 in AKI and its mechanism of regulating macrophage dynamics and functions remain unclear.

In this study, we have developed a FoxO1 inhibitor AS1842856-encapsulated liposome (referred to as AS-Lipo) and have demonstrated its effectiveness in mitigating I/R-induced renal injury. Additionally, we have generated mice with myeloid-specific conditional FoxO1 deletion (Lyz2-Cre^{ERT2} *FoxO1*$^{flox/flox}$) and have observed that the absence of FoxO1 in myeloid cells protects against I/R-induced kidney injury. Furthermore, our findings indicate that FoxO1 plays a crucial role in macrophage chemotaxis, inflammation, and migration, suggesting its potential as a promising therapeutic target and biomarker for AKI.

2. Materials and methods

2.1. Mice

Wild-type (WT) C57BL/6 male mice were purchased from the Animal Center of Peking University (Beijing, China). *FoxO1*$^{flox/flox}$ mice (C57BL6/J background) were kind gifts from Dr. Ming Li (Memorial Sloan-Kettering Cancer Center, New York, NY, USA), Lyz2-Cre^{ERT2} mice (C57BL6/J background) were from Gempharmatech Co., Ltd. (Nanjing, China). *FoxO1*$^{flox/flox}$ mice were crossed with Lyz2-Cre^{ERT2} mice to get Lyz2-Cre^{ERT2} *FoxO1*$^{flox/flox}$ mice. The resulting progenies of mice were genotyped by polymerase chain reaction (PCR) analysis of mouse tail genomic DNA. Tamoxifen (Solarbio, Beijing, China) was dissolved in corn oil, and mice were injected with 75 mg/kg daily for five consecutive days to activate Cre^{ERT2}. All mice were maintained in a pathogen-free animal facility in accordance with the National Institute of Health Guide for Care and Use of Laboratory Animals. Male mice aged 8−12 weeks were used for all studies. Age-matched and sex-matched littermate mice were used as controls. Animal experiments were approved by the Biomedical Ethics Committee of Peking University (LA 2016-212) and were in compliance with institutional guidelines.

2.2. Renal I/R injury models

An established mouse model of renal I/R injury was performed as described previously[18]. Briefly, after mice were anesthetized with an intraperitoneal injection of pentobarbital (60 mg/kg), the right renal was removed, and the left renal artery and vein were identified and clamped for 35 min with a non-traumatic clamp. Then, the clamp was released, and reperfusion was observed for 5 min to ensure the reflow process. The incision was then closed, and the animal was allowed to recover. During the ischemic period, body temperature was maintained at 37 °C using a temperature-controlled heating system. After reperfusion at 24, 48, and 72 h, blood samples and kidneys were collected for subsequent analysis.

To investigate the effect of AS-Lipo on I/R-induced injury, mice were injected with AS-Lipo in the tail vein (intravenous), a dose of 5 mg/kg, 24 h prior to renal I/R injury. Then, mice were intravenously injected with a dose of 5 mg/kg AS-Lipo once a day for two consecutive days beginning at 24 h post-renal I/R injury.

2.3. Lipopolysaccharide (LPS)-induced AKI models

Mice were injected intraperitoneally with 20 mg/kg LPS (Sigma−Aldrich, Darmstadt, Germany) to establish an *in vivo* AKI model. A saline solution was administered to the control mice. After LPS injection at 12 and 24 h, blood samples and kidneys were collected for subsequent analysis.

2.4. Renal function

Blood was collected from mice at 0, 24, 48, and 72 h after the induction of renal I/R injury. Serum creatinine and blood urea nitrogen (BUN) levels were measured by commercial kits (Nanjing Jiancheng Bioengineering Institute, Nanjing, China).

2.5. Haematoxylin and eosin (HE) staining

Kidneys were fixed with 4% formaldehyde, embedded in paraffin, and sectioned into 4 μm-thick. The sections were stained by hematoxylin and eosin for histological examination. The degree of tubular necrosis was scored using the semi-quantitative scores developed by Paller et al[24].

2.6. Immunofluorescence

For immunofluorescence staining, kidney tissues were embedded in Tissue-Tek O.C.T. Compound (Sakura Finetek, Tokyo, Japan) and sectioned into 4 μm-thick. Frozen sections were stained with primary antibodies, followed by staining with 4,6-diamidino-2-phenylindole. APC-labeled secondary antibodies (Zhong Shan-Golden Bridge Biological Technology Co., Ltd., Beijing, China) and FITC-labeled secondary antibodies (Zhong Shan-Golden Bridge Biological Technology Co., Ltd.) were used. Images were captured using a confocal microscope (Leica Microsystems, Wetzlar, Germany) and analyzed using ImageJ v1.8.0 Software.

2.7. Immunohistochemistry

Kidney paraffin sections were deparaffinized, rehydrated, and then incubated with an anti-CD68 antibody (Abcam, Boston, USA) at 4 °C overnight after heating-induced antigen retrieval in 0.01 mol/L citrate buffer. A secondary antibody (Jackson ImmunoResearch Laboratories, Pennsylvania, USA) was used to incubate for 45 min at room temperature. Then 3,3′-diaminobenzidine solution (Biorigin, Beijing, China) was applied for development. Finally, the sections were counterstained with haematoxylin and mounted.

2.8. Cell culture and treatments

The murine fibroblast L929 cells and RAW264.7 cells were purchased from the Cell Culture Centre, Institute of Basic Medical Science Chinese Academy of Medical Sciences (Beijing, China). RAW264.7 cells were maintained in Dulbecco's modified Eagle's medium (DMEM) (Macgene, Beijing, China), supplemented with 10% fetal bovine serum (FBS) and 1% penicillin/streptomycin in a humidified atmosphere of 5% CO_2 at 37 °C. Mouse renal tubular epithelial cells (mRTECs) were purchased from the BeNa Culture Collection (Xinyang, China). mRTECs were cultured in Roswell Park Memorial Institute (RPMI) 1640 medium (Macgene) supplemented with 10% FBS and 1% penicillin/streptomycin. Human umbilical vein endothelial cells (HUVECs) were purchased from Lifeline Cell Technology (Frederick, USA). HUVECs were maintained in vascular endothelial growth factor medium (Lifeline Cell Technology) supplemented with 2% FBS in a humidified atmosphere of 5% CO_2 at 37 °C.

For FoxO1 inhibition, AS1842856 (Selleck Chemicals, Houston, USA) was co-incubated with cells in doses of 0.01, 0.1, 1, 10, 100, and 1000 μmol/L.

2.9. Isolation of peritoneal macrophages and bone marrow-derived macrophages (BMDMs)

Mice were injected intraperitoneally with 2 mL of thioglycolate medium (3%) to induce macrophage recruitment into the peritoneal cavity. Cells were isolated from the peritoneal lavage and cultured in RPMI 1640 medium supplemented with 10% FBS and 1% penicillin/streptomycin. Femurs of mice were removed to isolate the primary BMDMs. Medullary cavities were flushed with cold phosphate-buffered saline (PBS) buffer, and the resulting suspension was removed red blood cells by lysis buffer. Cells were cultured in DMEM containing 30% L929 cell conditioned medium, 10% FBS, and 1% penicillin/streptomycin for 7 days. For *in vitro* polarization, a pro-inflammatory macrophage polarization by culturing BMDMs with 100 ng/mL LPS and 20 ng/mL interferonγ (IFNγ) for 24 h, and an anti-inflammatory macrophage polarization by culturing BMDMs with 20 ng/mL interleukin4 (IL4) for 24 h.

For FoxO1 overexpression, adenovirus-expressing mice FoxO1 (Ad-FoxO1) were used to transfect BMDMs. For ARHGEF1 inhibition, ARHGEF1 siRNA (Beijing Tsingke Biotech Co., Ltd., Beijing, China) or scramble siRNA with jetPRIME® transfection reagent (Polyplus-transfection, Illkirch, France) were used to transfect BMDMs. For ARHGEF1 inhibition and FoxO1 overexpression, BMDMs were treated with si-ARHGEF for 24 h first and then with fresh media containing Ad-FoxO1 for another 24 h.

2.10. AS-Lipo preparation

AS-Lipo was prepared by using a thin film-hydration method[25]. Briefly, AS1842856, lecithin, cholesterol, and DSPE-PEG_{2000} at the mass ratio of 1:30:3:3 were dispersed in methanol/chloroform (1/1, *v/v*), and then the thin film of lipid was formed by removing organic solvents under vacuum using a rotary evaporator. The thin film was hydrated by PBS buffer at a slow rate in the water bath. The thus-formed liposomes were extruded through 0.4 and 0.2 μm

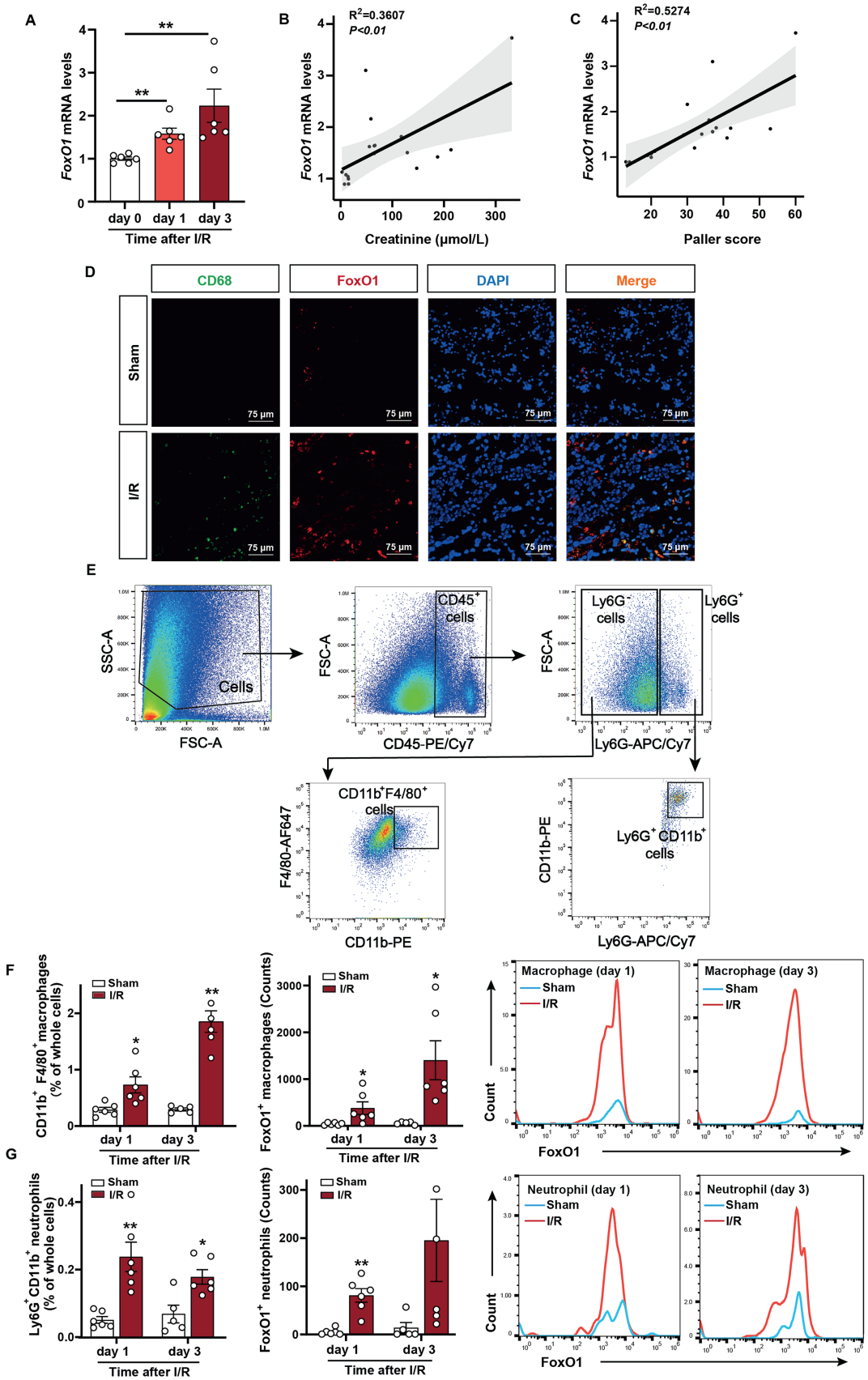

Figure 1 FoxO1 was elevated in renal macrophages in I/R injury mice. (A) The mRNA expression levels of *FoxO1* were measured in WT mice on Day 1 and Day 3 after renal I/R injury by qPCR ($n = 6$). (B, C) Correlations between renal *FoxO1* mRNA expression levels and serum

nucleopore polycarbonate membranes using Avati LiposoFast (Avanti Polar Lipids, Inc., Birmingham, USA) and then maintained at 4 °C.

2.11. *In vitro cellular uptake assay*

The HUVECs, mRTECs, or BMDMs were seeded in 12 well plates and cultured for 24 h. The AS-Lipo was added to the cells for 2 h incubation, respectively. Then, the cells were collected and detected by flow cytometry with NovoCyte Flow Cytometer Systems (Agilent, CA, USA).

2.12. *Biodistribution of AS-Lipo*

The DIR-labeled AS-Lipo was administered intravenously into the mice, and then the mice established renal I/R injury models. The biodistribution of AS-Lipo was monitored using an IVIS imaging system (Caliper PerkinElmer, Hopkinton, USA) at the predetermined time points (6, 12, 24 and 48 h). At the experimental endpoint, the mice were sacrificed, and their heart, liver, spleen, lung, and kidney tissues were harvested for *ex vivo* imaging.

2.13. *Isolation of renal immune cells*

Renal immune cells were isolated from the renal by collagenase digestion and differential centrifugation using Percoll (Solarbio). Kidneys were digested in RPMI 1640 containing 100 μg/mL DNase I (Solarbio) and 1 mg/mL collagenase IV (Solarbio) for 45 min at 37 °C with gentle shaking. After digestion, cells were passed through a 70 and 40 μm cell strainer (BD Life Sciences, NJ, USA) to obtain single-cell suspension. Then, single cells were subject to gradient centrifugation using 72% and 36% Percoll. Immune cells were enriched at the 36%−72% interface and were collected.

2.14. *Flow cytometry*

Renal single-cell suspension was centrifuged at 300 × *g* for 5 min at 4 °C and resuspended in PBS buffer containing 1% bovine serum albumin (BSA). Cells were incubated with fluorophore-conjugated primary antibodies for 30 min. Antibodies employed in these studies included CD45 (PE/Cyanine7), Ly6G (APC-Cyanine7), F4/80 (Alexa Fluor 647), CD11b (PE), CD31 (FITC), Ly6C (Brilliant Violet 421) and FoxO1 (Alexa Fluor 488). Following incubation with primary antibodies, cells were incubated with secondary antibodies. After washing twice with PBS buffer containing 1% BSA, the cells were subjected to analysis on a Gallios flow cytometer (Beckman Coulter, CA, USA). The flow cytometry results were analyzed using FlowJo™ v10.8 Software (BD Life Sciences).

2.15. *Enzyme-linked immunosorbent assay (ELISA)*

Blood was collected from mice 24 h after induction of renal I/R injury, and culture supernatant of BMDMs was collected and centrifuged at 300 × *g* for 10 min to remove cellular debris. Then, the level of IL1β and IL6 in serum or culture supernatant was measured according to the manufacturer's instructions (Biolegend, USA). One day prior to running the ELISA, capture antibody solution was added to a 96-well plate and incubated overnight at 4 °C. The plate was washed; standards or samples were added to wells, and incubated at room temperature for 2 h with shaking. The plate was washed, diluted detection antibody solution was added to wells, and incubates at room temperature for 1 h with shaking. The plate was washed, diluted Avidin-HRP solution was added to wells, and incubated at room temperature for 30 min with shaking. The plate was washed again, freshly mixed TMB substrate solution was added, and incubated in the dark for 15 min. The reaction was stopped by adding stop solution to the wells. The absorbance was read at 450 nm.

2.16. *In vitro migration assay*

Transwell assay was used to assess cell migration[26]. BMDMs from mice (100,000 cells) were seeded in the upper chamber of a 24-well PET membrane (8 μm pore size; Corning, New York, USA). Cells transferred to the lower chamber in response to 10% FBS, 100 ng/mL Chemokine (CC-motif) ligand 19 (CCL19) (R&D Systems, Minnesota, USA), 100 ng/mL CCL21 (R&D Systems), 100 ng/mL C−X3−C motif chemokine ligand 1 (CX3CL1) (R&D Systems) or 250 mmol/L f-Met−Leu−Phe (fMLP) (Sigma−Aldrich) for 3 h. Cells in the upper chamber were removed with a cotton swab, and the filters were fixed with 4% paraformaldehyde and stained with crystal violet. Filters were photographed using a microscope (Leica Microsystems) and cell number was counted.

2.17. *Cell migration trajectory assay*

For long-term live-cell imaging, RAW264.7 cells were plated on PA gel and maintained in CO_2-independent DMEM (ThermoFisher Scientific, MA, USA) supplemented with 10% FBS and 1% penicillin/streptomycin at 37 °C throughout the imaging process. Bright-field images for migration analysis were acquired with a 10 × objective lens on Olympus IX83. Acquisitions were performed at 15-min intervals over 12 h. Images were analyzed using the 'Manual Tracking' and 'Chemotaxis Tool' plugins of Fiji. Coordinates and distances of cell movement were tracked using the 'Manual Tracking' plugin of Fiji, and then tracking data were imported into the 'Chemotaxis Tool' plugin to generate statistic features such as distance and velocity.

2.18. *RhoA activation assay*

After treatment with 200 nmol/L AS1842856 or Ad-FoxO1 for 24 h, RAW264.7 cells were harvested and extracted with radio immunoprecipitation assay buffer containing protease inhibitors Cocktail (MedChemExpress, Shanghai, China). After centrifugation, protein supernatants were collected. RhoA activity was assessed with the instructions of Rhotekin-RBD Beads (Cytoskeleton, Denver, USA). Loading Buffer and GTPγS were added to the protein supernatants, and incubated at room temperature for 15 min. The reaction was stopped by adding StopBuffer.

creatinine or Paller score after renal I/R injury ($n = 18$). (D) Representative immunofluorescence staining for FoxO1 and CD68 in kidney sections of renal I/R injury mice on Day 1. Scale bar, 75 μm. (E) Gating strategy of flow cytometry in kidney tissues on Day 1 and Day 3 after renal I/R injury. (F) Flow cytometric analysis shows the percent of renal macrophages and the number of FoxO1-positive macrophages ($n = 5$−6). (G) Flow cytometric analysis shows the percent of renal neutrophils and the number of FoxO1-positive neutrophils ($n = 5$−6). Data are represented as mean ± SEM. *$P < 0.05$, **$P < 0.01$.

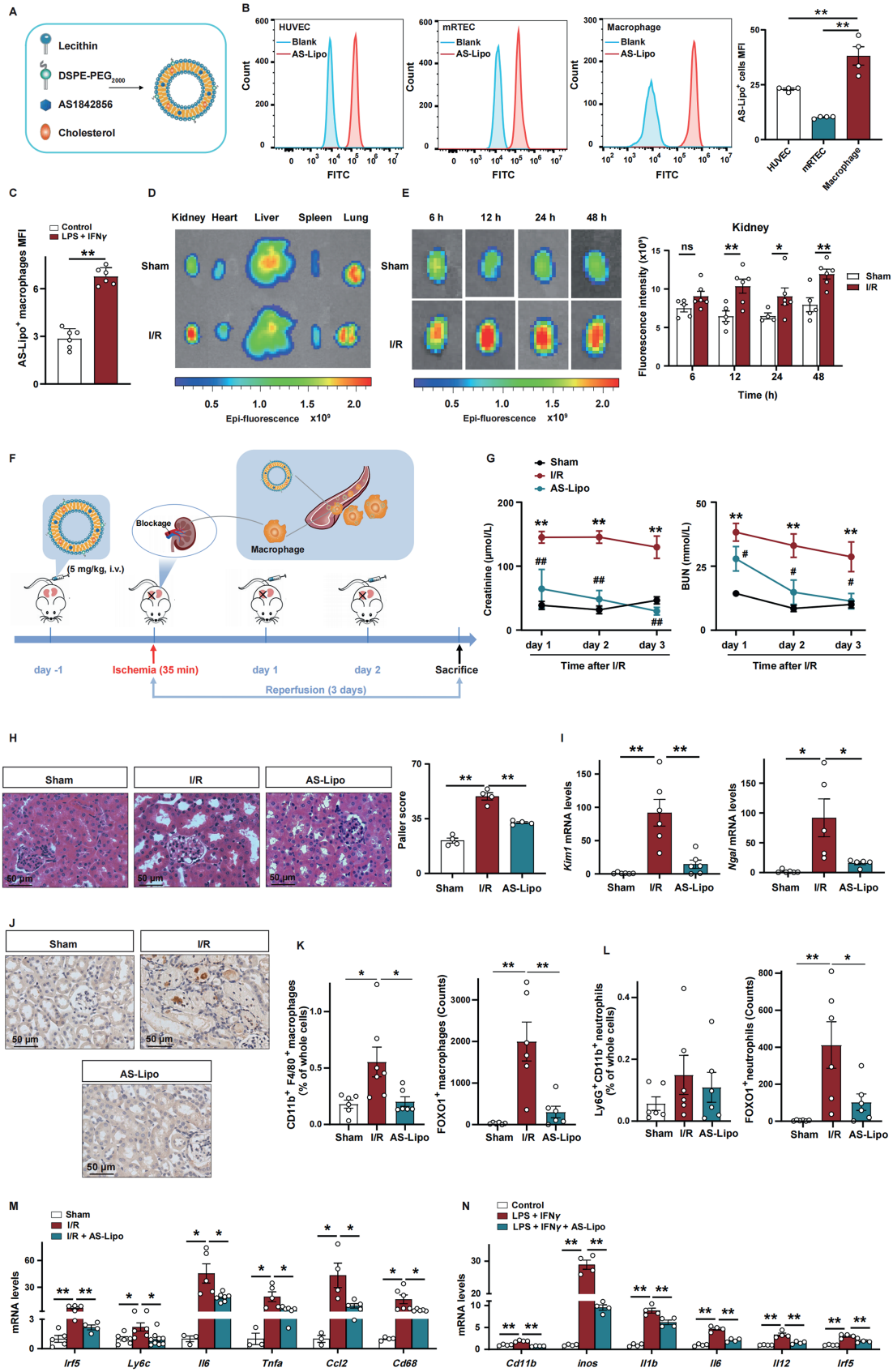

Figure 2 AS-Lipo protected against renal I/R-induced AKI. (A) Schematic illustration shows the preparation of AS-Lipo. (B) Uptake of FITC-labeled AS-Lipo by HUVECs, mRTECs, and BMDMs *in vitro* and mean fluorescence intensity (MFI) of cell uptake capability ($n = 4$). (C) Uptake of DID-labeled AS-Lipo by BMDMs, LPS, and IFNγ treated BMDMs *in vitro* and MFI of cell uptake capability ($n = 6$). (D) *Ex vivo*

Rhotekin-RBD protein beads were resuspended and protein-bound beads were added to each sample. The tubes were gently rotated at 4 °C for 1 h. The beads were pelleted by centrifugation at 7000 × *g*, 4 °C for 1 min. The supernatant was removed and the beads were washed. After pelleted by centrifugation, the beads were resuspended in the sodium dodecyl sulfate sample buffer. The bead and supernatant samples can be analyzed by Western blotting using Anti-Rho monoclonal antibody (Cytoskeleton).

2.19. Terminal deoxynucleotidyl transferase dUTP nick-end labeling (TUNEL) assay

TUNEL staining utilizes the ability of the enzyme terminal deoxynucleotidyl transferase to incorporate labeled dUTP onto the free 3′-hydroxyl termini of fragmented genomic DNA. Apoptotic kidney tissues and mRTECs were examined according to the instructions of the TUNEL Assay Kit (Promega, Madison, WI, USA).

2.20. Quantitative PCR (qPCR)

Total RNAs were isolated using Trizol reagent (ThermoFisher Scientific). RevertAid First Strand cDNA Synthesis Kit (ThermoFisher Scientific) was used to synthesize cDNA from total RNAs. qPCR was performed according to the following reaction system: 2 μL primers, 2 μL cDNA, 6 μL nuclease-free water, and 10 μL SYBR Green Real-Time PCR Master Mix (ThermoFisher Scientific). Relative mRNA levels were calculated with the $2^{-\Delta\Delta Ct}$ method. The specific primers used are shown in Supporting Information Table S1.

2.21. Chromatin immunoprecipitation (ChIP)-qPCR

RAW264.7 cells were maintained in DMEM supplemented with 10% FBS and treated with AS1842856 before harvest. Cells were fixed with 4% paraformaldehyde and then resuspended with lysis buffer containing protease inhibitors Cocktail. The lysates were subjected to ultrasonication (3 s on and 3 s off, 20 cycles) and centrifuged at 14,000 × *g* for 10 min The fragmented chromatin was immunoprecipitated with anti-FoxO1 antibody (Cell Signaling Technology) or control IgG (Santa Cruz Biotechnology, Dallas, USA) and then captured using protein G agarose beads (ThermoFisher Scientific). Chromatin was eluted from the beads and treated with proteinase K, which was then followed by phenol/chloroform extraction and ethanol precipitation to obtain purified DNA. The DNA samples were used as the template for ChIP-qPCR.

2.22. Western blot

Proteins from the kidney tissues or cells were extracted with radio immunoprecipitation assay buffer containing protease inhibitors Cocktail. After centrifugation, protein supernatants were collected. Total protein concentration was quantified with the Bicinchoninic Acid Assay kit (ThermoFisher Scientific). Equal protein amounts were separated by SDS-polyacrylamide gel electrophoresis and transferred onto polyvinylidene difluoride immobilon-P membranes. Membranes were blocked in blocking buffer (Tris-buffered saline plus 0.05% Tween-20 and 5% BSA) for 1 h, and then incubated overnight at 4 °C with primary antibodies. After incubation with the appropriate HRP-conjugated secondary antibody, blots were developed with electrochemiluminescence reagent (Santa Cruz Biotechnology). The primary antibodies used are shown in Supporting Information Table S2. The staining intensity of bands was determined by ImageJ (Version 1.8.0, USA).

2.23. RNA sequencing and raw data analysis

The library preparation and sequencing were performed at the Annoroad Gene Technology Co., Ltd. (Beijing, China). Briefly, sequencing libraries were generated using NEBNext® Ultra™ RNA Library Prep Kit for Illumina® (CA, USA) following the manufacturer's recommendations, and index codes were added to attribute sequences to each sample. The clustering of the index-coded samples was performed on a cBot cluster generation system using HiSeq PE Cluster Kit v4-cBot-HS (Illumina) according to the manufacturer's instructions. After cluster generation, the libraries were sequenced on an Illumina NovaSeq 6000 platform, and 150 bp paired-end reads were generated. RNA sequencing reads data were demultiplexed with Illumina's bcl2fastq2 and were then aligned to the *Mus musculus* Ensembl release 76 top-level assembly with HISAT2 version 2.1.0. Reads Count for each gene in each sample was counted by HTSeq v0.6.0, and fragments per kilobase of transcript per millon mapped reads (FPKM) were then calculated to estimate the expression level of genes in each sample. RNA sequencing downstream data analysis mainly includes differentially expressed gene (DEG) analysis; gene set variation analysis (GSVA), gene ontology (GO) function enrichment, and gene set enrichment analysis (GSEA). The whole analysis process was completed with R software (version number: 4.10) and the corresponding R package. The differential genes between different experimental groups were calculated with the DESeq2 package, and adjusted $P < 0.05$ and $|\log_2 FC|>1$ were selected as the screening criteria. Each sample was scored with 50 Hallmark gene sets GSVA through the GSVA package, and all

fluorescence images of excised organs after tail vein injection of AS-Lipo. (E) *Ex vivo* fluorescence images and MFI of kidney tissues after tail vein injection of AS-Lipo ($n = 4-6$). (F) Schematic illustration shows the AS-Lipo administration procedure for renal I/R injury mice. Mice were intravenously injected with AS-Lipo 24 h before renal I/R injury and once a day for two consecutive days beginning at 24 h post-renal I/R injury. (G) Serum creatinine and BUN levels in the indicated mouse groups ($n = 5-6$). $^{**}P < 0.01$ *versus* sham, $^{\#}P < 0.05$ *versus* I/R, $^{\#\#}P < 0.01$ *versus* I/R. (H) Representative images of HE staining of kidney sections and tubular injury of the kidneys quantified by Paller score from different groups of mice on Day 3 after renal I/R injury ($n = 4$). Scale bar, 50 μm. (I) Renal *Kim1* and *Ngal* mRNA expression levels from different groups of mice on Day 3 after renal I/R injury ($n = 5-6$). (J) Representative immunohistochemistry staining for CD68 in kidney sections from different groups of mice on Day 1 after I/R injury. Scale bar, 50 μm. (K) Flow cytometric analysis shows the percent of renal macrophages and the number of FoxO1-positive macrophages ($n = 6-7$). (L) Flow cytometric analysis shows the percent of renal neutrophils and the number of FoxO1-positive neutrophils ($n = 6$). (M) The mRNA expression levels of the inflammatory gene in the kidney on Day 3 after I/R injury ($n = 3-6$). (N) The mRNA expression levels of the inflammatory gene in LPS and IFNγ treated BMDMs ($n = 4$). Data are represented as mean ± SEM. ns, no significance; $^{*}P < 0.05$, $^{**}P < 0.01$.

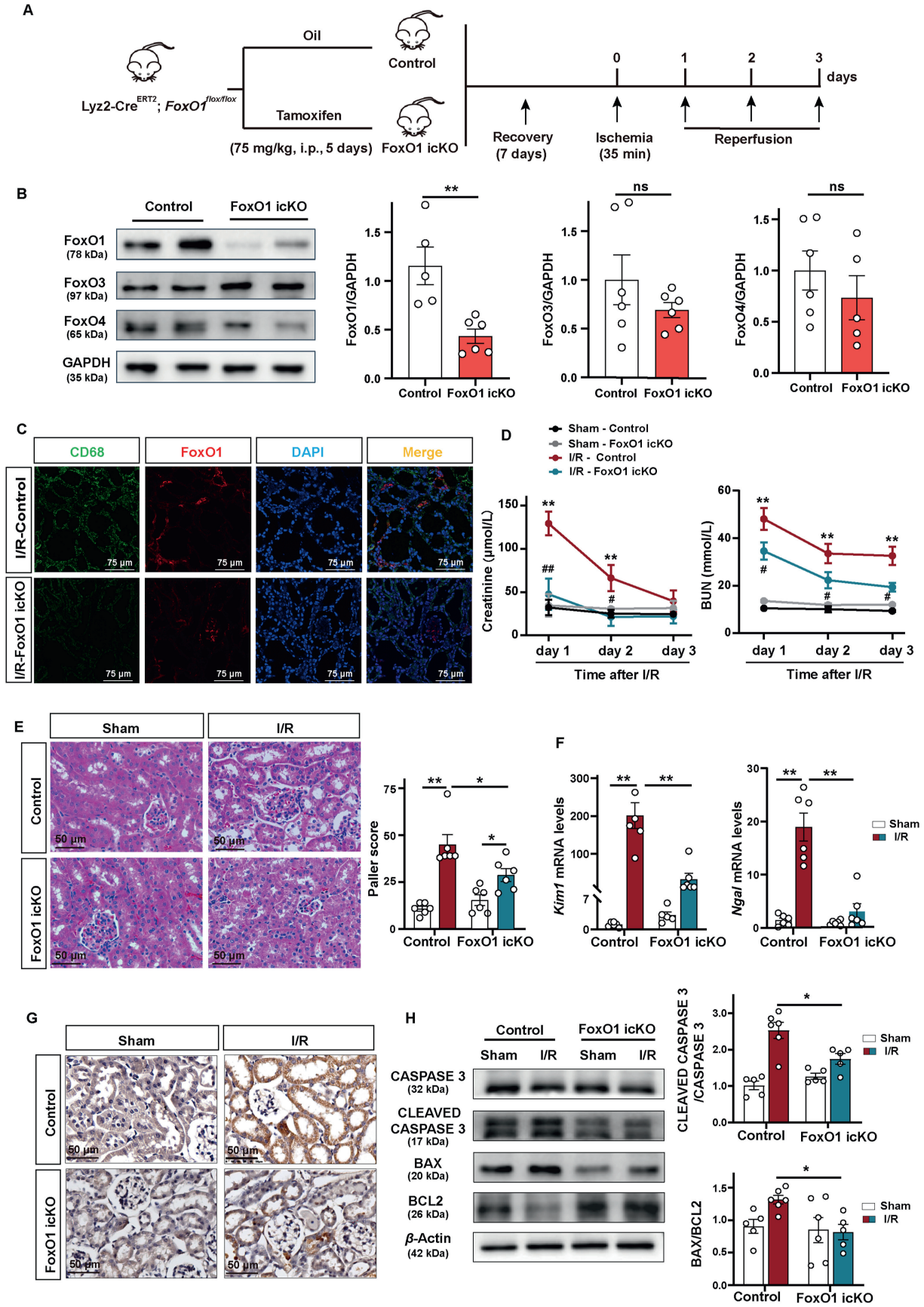

Figure 3 Myeloid FoxO1 deletion protected against renal I/R-induced AKI. (A) The schematic diagram shows the procedure of renal I/R injury for knockout mice. (B) Peritoneal macrophages were isolated and cultured, followed by Western blotting analysis of the protein levels of FoxO1,

enrichment pathways with differences were clustered by Cytoscape software according to different biological characteristics. GO and GSEA function enrichment analysis of DEGs completed and visualized in g: Profiler online database (https://biit.cs.ut.ee/gprofiler/gost).

2.24. Statistical analysis

All animal studies were performed after randomization. All data are expressed as the mean ± standard error of mean (SEM). Statistical analyses were conducted in GraphPad Prism 9.0. Kolmogorov−Smirnov's test was used to determine normality. The statistical differences between groups were evaluated by unpaired Student's *t*-test. When more than two treatment groups were compared, ANOVA with Tukey's test was used when the *F* statistic was significant, and there was no significant variance in homogeneity. Differences were considered to be statistically significant at $P < 0.05$.

3. Results

3.1. FoxO1 was upregulated in renal macrophages after I/R injury

Four distinct isoforms of FoxO (FoxO1, FoxO3, FoxO4, and FoxO6) have been identified in mammals, with all isoforms expressed in renal tissue except for FoxO6[27]. To assess the potential involvement of FoxO isoforms in the development of I/R-induced AKI, we examined the expression of FoxO1, FoxO3, and FoxO4 in kidney tissue. The mRNA levels of *FoxO1* in the kidney exhibited a gradual increase in the days following I/R injury (Fig. 1A). The results of the correlation analysis demonstrated a significant association between renal *FoxO1* mRNA levels and both serum creatinine levels and the extent of tubular necrosis following I/R injury (Fig. 1B and C). Conversely, *FoxO3* mRNA levels exhibited a decrease after I/R injury (Supporting Information Fig. S1A). Notably, no correlation was observed between *FoxO3* mRNA levels and serum creatinine levels, although a negative correlation was found between *FoxO3* mRNA levels and the extent of tubular necrosis following I/R injury (Fig. S1B and S1C). Besides, it was observed that the levels of *FoxO4* mRNA were unaffected by I/R injury (Fig. S1D−S1F).

One day after I/R-induced AKI, protein levels of FoxO1 in the $CD68^+$ macrophages were significantly higher in the I/R group compared with the sham group (Fig. 1D). Nonetheless, FoxO3 or FoxO4 levels in the $CD68^+$ macrophages were not different between the two groups (Fig. S1G and S1H). Given that macrophages and neutrophils are the predominant myeloid cell types involved in renal inflammation and repair during I/R-induced AKI[28], flow cytometry analysis was explored to investigate the expression of renal FoxO1 on macrophages and neutrophils in mice with renal I/R injury (Fig. 1E). The results showed that renal I/R injury resulted in an elevation of $CD45^+Ly6G^-CD11b^+F4/80^+$ macrophages and FoxO1-positive macrophages (Fig. 1F). Additionally, an increase in $CD45^+Ly6G^+CD11b^+$ neutrophils and FoxO1-positive neutrophils following I/R injury was found (Fig. 1G). These results collectively suggest a strong association between the rise in macrophage FoxO1 levels and AKI in the renal I/R injury mouse model.

3.2. AS-Lipo protected against I/R-induced AKI

Liposomes naturally target cells of the mononuclear phagocytic system, particularly macrophages[29]. Here, we prepared AS-Lipo using a thin-film hydration technique (Fig. 2A). The cellular uptake profiles of AS-Lipo were determined quantitatively by flow cytometry. As shown in Fig. 2B, BMDMs exhibited a higher uptake of AS-Lipo compared to mRTECs and HUVECs. Moreover, pro-inflammatory macrophages showed significantly higher uptake of AS-Lipo compared to native macrophages (Fig. 2C). For the following *in vivo* experiment, the biodistribution of AS-Lipo was explored in the renal I/R injury mice model. After intravenous injection of AS-Lipo, the I/R model was used, and the distribution of AS-Lipo containing DIR near-infrared dye was visualized. As shown in Fig. 2D and Supporting Information Fig. S2A−S2E, in the sham group, AS-Lipo was mainly accumulated in the liver and lung tissue, less in the kidney tissue. Notably, I/R injury significantly increased AS-lipo's distribution in the kidney tissue. Further analysis indicated that renal AS-Lipo in the I/R group was significantly higher than the sham group at different time points, including 12, 24, and 48 h (Fig. 2E). Furthermore, the uptake rates of AS-Lipo in various cell types *in vivo* with I/R injury were detected using flow cytometry. As shown in Fig. S2F, macrophages showed a higher uptake of AS-Lipo compared to neutrophils and endothelial cells.

Next, the impact of AS-Lipo on I/R-induced AKI was examined (Fig. 2F). In the I/R-induced AKI model, AS-Lipo significantly reduced serum creatinine and BUN levels (Fig. 2G). I/R injury resulted in severe kidney injury, evident by tubular brush border dilatation and loss in the proximal tubular[30]. The administration of AS-Lipo reduced I/R-induced tubular damage (Fig. 2H). Additionally, the levels of kidney injury molecule 1 (Kim1) and neutrophil gelatinase-associated lipocalin (Ngal), two established biomarkers of AKI, were significantly up-regulated in the I/R injury group but reduced in the AS-Lipo group (Fig. 2I).

Furthermore, AS-Lipo exhibited a decrease in the infiltration of $CD68^+$ macrophages induced by I/R injury (Fig. 2J). Flow cytometry results showed that AS-Lipo decreased an elevation of $CD45^+Ly6G^-CD11b^+F4/80^+$ macrophages and FoxO1-positive macrophages induced by I/R injury (Fig. 2K). Additionally, it was observed that the number of $CD45^+Ly6G^+CD11b^+$ neutrophils has no difference between these three groups. However, an increase in FoxO1-positive neutrophils following I/R injury was inhibited by AS-Lipo (Fig. 2L). Further analysis showed that AS-Lipo downregulated the expression of pro-inflammatory macrophage-associated genes induced by I/R injury (Fig. 2M). Simultaneously, the expression of anti-inflammatory macrophage-associated genes was

FoxO3, and FoxO4 ($n = 5-6$). (C) Representative immunofluorescence staining for FoxO1 and CD68 in kidney sections of renal I/R injury mice on Day 1. Scale bar, 75 μm. (D) Serum creatinine and BUN levels in the indicated mouse groups ($n = 5-6$). $^{**}P < 0.01$ *versus* sham-control, $^{\#}P < 0.05$ *versus* I/R-control, $^{\#\#}P < 0.01$ *versus* I/R-control. (E) Representative images of HE staining of kidney sections and tubular injury of the kidneys were quantified by Paller score from different groups of mice on Day 3 after renal I/R injury ($n = 6$). Scale bar, 50 μm. (F) Renal *Kim1* and *Ngal* mRNA expression levels from different groups of mice on Day 3 after renal I/R injury ($n = 5-6$). (G) Representative images of TUNEL staining in kidneys of renal I/R injury mice on Day 1. Scale bar, 50 μm. (H) The protein levels of Caspase 3, Cleaved Caspase 3, BAX, and BCL2 in kidneys of renal I/R injury mice on day 3 were detected by Western blotting ($n = 5-6$). Data are represented as mean ± SEM. ns, no significance; $^{*}P < 0.05$, $^{**}P < 0.01$.

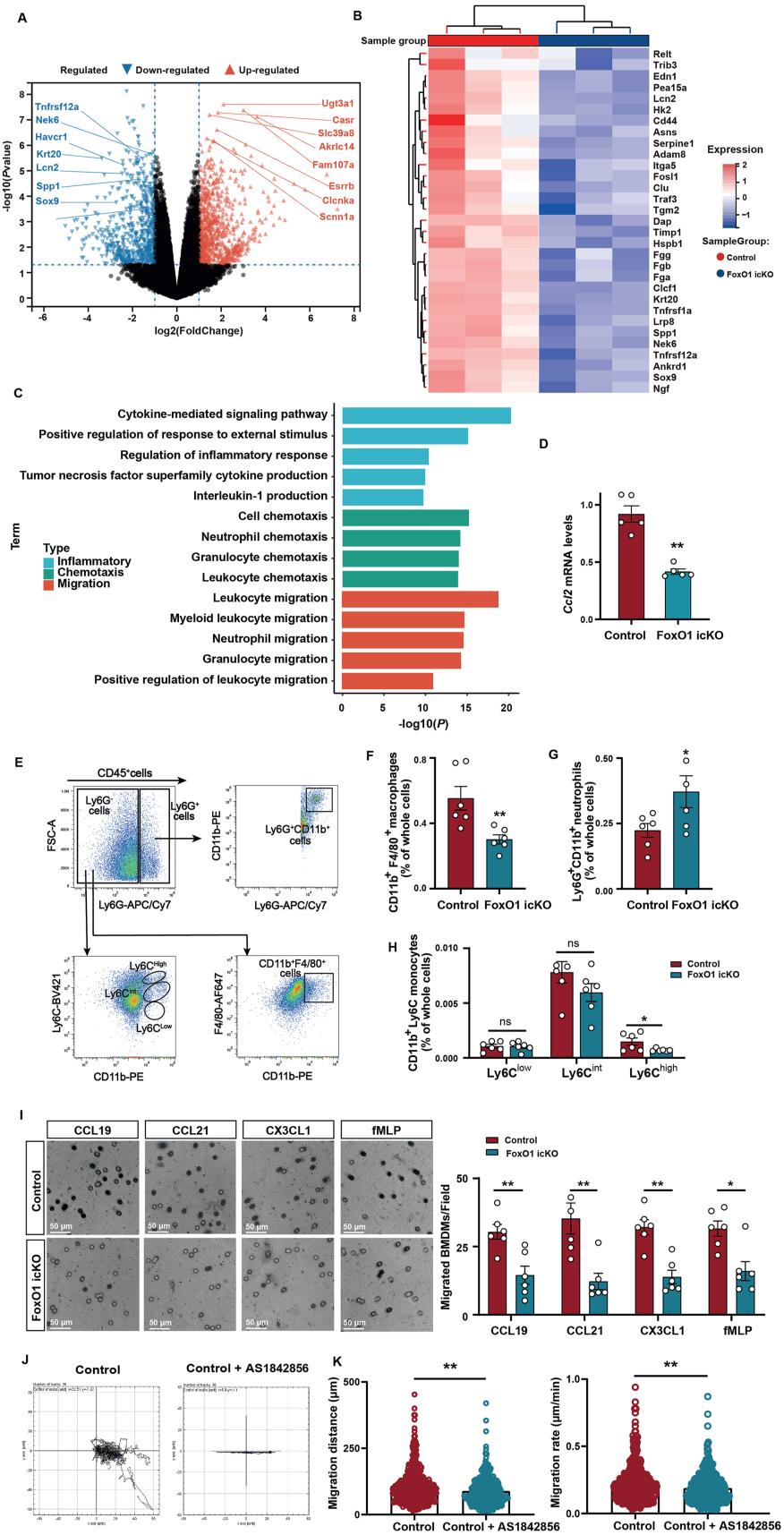

Figure 4 Myeloid FoxO1 depletion inhibited macrophage chemotaxis and migration. (A) Volcano plot of DEGs in kidney tissues of renal I/R injury mice on Day 1. (B) Heatmap for common DEGs associated with apoptosis in kidney tissues of renal I/R injury mice on Day 1. (C) GO

inhibited by AS-Lipo, as demonstrated in Fig. S2G. *In vitro*, AS-Lipo reduced the expression of pro-inflammatory macrophage-associated genes in BMDMs isolated from WT mice and treated with LPS and IFNγ, as shown in Fig. 2N. Following IL4 treatment, AS-Lipo also decreased the expression of anti-inflammatory macrophage-associated genes in BMDMs (Fig. S2H). These findings suggest that AS-Lipo effectively ameliorates functional and histological renal injury induced by I/R injury.

3.3. Myeloid FoxO1 deficiency protected against I/R-induced AKI

The utilization of inducible Cre-ERT recombinase represents a gene-targeting approach that enables researchers to manipulate gene expression in a time-dependent manner, frequently employed in the generation of conditional knockout mice[31,32]. We generated Lyz2-Cre^{ERT2} *FoxO1*$^{flox/flox}$ mice with a specific knockout of FoxO1 in myeloid cells and utilized an I/R-induced AKI model to investigate its effects (Fig. 3A). The genotyping of mice was confirmed through PCR analysis of genomic DNA extracted from mouse tail samples (Supporting Information Fig. S3A). Peritoneal macrophages obtained from Lyz2-Cre^{ERT2} *FoxO1*$^{flox/flox}$ mice exhibited a significant reduction in FoxO1 expression (Fig. 3B). Immunofluorescent analysis revealed a substantial decrease in FoxO1 expression in CD68^{+} macrophages in mice with myeloid FoxO1 deficiency (Fig. 3C). Consistently, myeloid FoxO1 deficiency mice subjected to renal I/R injury demonstrated notable improvements in renal function (Fig. 3D) and tubular injury (Fig. 3E). A significant reduction in the levels of *Kim1* and *Ngal* was observed in mice with myeloid FoxO1 deficiency and I/R injury (Fig. 3F). Furthermore, we found that myeloid FoxO1 deficiency led to a decrease in the infiltration of CD68^{+} macrophages induced by I/R injury (Fig. S3B).

The TUNEL assay revealed an increase in TUNEL-positive staining in the kidneys following I/R injury, while myeloid FoxO1 deficiency resulted in a decrease in the percentage of TUNEL-positive cells (Fig. 3G). Moreover, I/R injury triggered the cleavage and activation of Caspase 3 compared to the sham group, but myeloid FoxO1 deficiency inhibited I/R-induced Caspase 3 activation (Fig. 3H). The anti-apoptotic protein BCL2 and pro-apoptotic protein BAX are frequently used as apoptotic markers in the mitochondrial pathway[33,34]. As shown in Fig. 3H, it is demonstrated that I/R injury increased BAX protein levels and decreased BCL2 protein levels. However, the absence of myeloid FoxO1 prevented the upregulation of the BAX/BCL2 ratio. These findings collectively suggest that myeloid FoxO1 deficiency offers protection against I/R-induced AKI.

3.4. FoxO1 inhibition reduced macrophage chemotaxis and migration

In the myeloid FoxO1 deficiency mice group, AKI-associated genes, such as SRY-box transcription factor 9 (Sox9), keratin 20 (Krt20), and hepatitis a virus cellular receptor 1 (Havcr1), were found to be significantly downregulated compared to the control group (Fig. 4A). Furthermore, the analysis of DEGs related to apoptosis in kidney tissues indicated that myeloid FoxO1 deficiency resulted in the downregulation of apoptotic genes (Fig. 4B). Additionally, the GO enrichment analysis revealed that the downregulated DEGs were associated with cell chemotaxis, migration, and inflammation (Fig. 4C). The qPCR analysis revealed significant inhibition of *Ccl2* mRNA expression in kidney tissues with renal I/R injury in the presence of myeloid FoxO1 deficiency (Fig. 4D). Flow cytometry analysis demonstrated the presence of infiltrating macrophages and neutrophils in kidney tissues on day 1 post-renal I/R injury (Fig. 4E). Notably, the percentage of CD45^{+}Ly6G^{-}CD11b^{+}F4/80^{+} macrophages was found to be lower in mice with myeloid FoxO1 deficiency (Fig. 4F), while an increased population of CD45^{+}Ly6G^{+}CD11b^{+} neutrophils was observed in the same group (Fig. 4G). Ly6C^{high} monocytes, which originate from the circulating system and are capable of responding to pro-inflammatory macrophages[35], were examined in this study. The results showed that the deficiency of myeloid FoxO1 significantly decreased the proportion of CD45^{+}Ly6G^{-}CD11b^{+} Ly6C^{high} monocytes while having no impact on Ly6C^{low} and Ly6C^{int} monocytes (Fig. 4H).

Additionally, the role of FoxO1 in macrophage chemotaxis was further investigated by examining the chemotactic responses of BMDMs in the absence of myeloid FoxO1. The migration assay demonstrated that the deficiency of myeloid FoxO1 inhibited the chemotactic responses of BMDMs when exposed to CCL19, CCL21, CX3CL1, and fMLP (Fig. 4I). Furthermore, the RAW264.7 cells were subjected to treatment with the FoxO1 inhibitor AS1842856, followed by an investigation into the potential role of FoxO1 in macrophage migration. As shown in Supporting Information Fig. S4A, the viability of RAW264.7 cells was unaffected by treatment with AS1842856 at concentrations ranging from 0.01 to 1000 μmol/L. Analysis of cell migration trajectories revealed significant inhibition of migration distance and migration rate in RAW264.7 cells treated with AS1842856, as depicted in Fig. 4J and K. It is worth noting that F-actin, a cytoskeletal protein associated with cell migration, was examined[36]. Fluorescence staining of F-actin indicated a reduction in actin cytoskeleton staining in RAW264.7 cells following treatment with AS1842856 (Fig. S4B).

3.5. FoxO1 regulated macrophage migration via ARHGEF1

After treatment with AS1842856, the protein−protein interaction (PPI) network of the DEGs expression of BMDMs was analyzed by using the STRING database (http://string-db.org) and Cytoscape. PPI network showed that DEGs were mainly enriched in protein targeting to membrane, extracellular matrix process and focal adhesion, cell death, metabolic pathway, and Rho regulation (Fig. 5A). GSEA indicated that the DEGs were enriched in processes related to the RhoA pathway (Fig. 5B). Heat map showed that AS1842856 treatment down-regulate RhoA pathway-associated genes (Fig. S4C). Subsequently, the levels of

enrichment analysis of genes in kidney tissues of renal I/R injury mice on Day 1. (D) Renal *Ccl2* mRNA expression levels of mice on Day 1 after renal I/R injury ($n = 5$). (E) Gating strategy of flow cytometry in kidney tissues on Day 1 after renal I/R injury. (F−H) Flow cytometric analysis shows the percent of renal macrophages, neutrophils, and Ly6C$^{low/int/high}$ monocytes in kidney tissues on Day 1 after renal I/R injury ($n = 5-6$). (I) Chemotactic responses to CCL19, CCL21, CX3CL1, and fMLP of BMDMs were determined by Transwell migration assay ($n = 5-6$). (J) Representative image of RAW264.7 cell migration trajectories after 200 nmol/L AS1842856 treatment. (K) Migration distance and rate of RAW264.7 cells after 200 nmol/L AS1842856 treatment. Data are represented as mean ± SEM. ns, no significance; *$P < 0.05$, **$P < 0.01$.

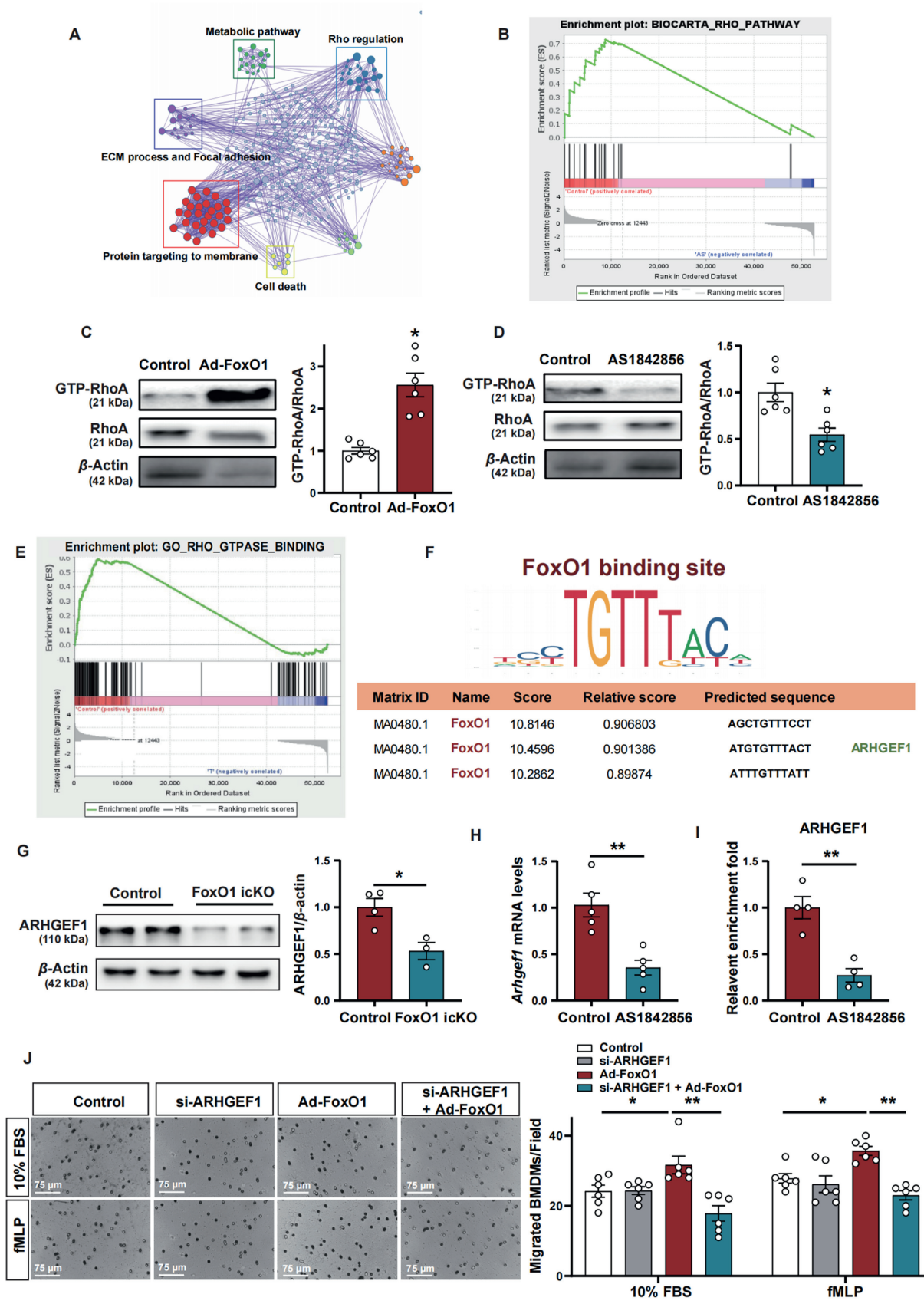

Figure 5 FoxO1 regulated macrophage migration *via* ARHGEF1. (A) PPI network of BMDMs after 200 nmol/L AS1842856 treatment. (B) GSEA of Rho pathway of BMDMs after 200 nmol/L AS1842856 treatment. (C, D) Representative Western blots and quantifications of GTP-RhoA and RhoA protein levels in RAW264.7 cells after Ad-FoxO1 or 200 nmol/L AS1842856 treatment ($n = 6$). (E) GSEA of Rho GTPase

GTP-RhoA (active RhoA) were assessed using Rhotekin-RBD Beads. As shown in Fig. 5C, the levels of GTP-RhoA exhibited an increase upon treatment with FoxO1 adenovirus (Ad-FoxO1). Conversely, a significant decrease in GTP-RhoA levels was observed following treatment with AS1842856 (Fig. 5D).

Activation of RhoA is facilitated by Rho-GTPase. GSEA demonstrated that AS1842856 effectively inhibits the expression of Rho-GTPase (Fig. 5E). The regulation of RhoA GTPase, crucial for cell migration, is mediated by ARHGEF1[37,38]. To investigate the interaction between FoxO1 and ARHGEF1, the JASPAR online tool was employed. It was observed that the promoter region of ARHGEF1 contains the FoxO1 binding motif, as depicted in Fig. 5F. Protein levels of ARHGEF1 were found to be lower in peritoneal macrophages from mice with myeloid FoxO1 deficiency, as shown in Fig. 5G. The real-time PCR analysis revealed that AS1842856 treatment resulted in a decrease in the mRNA expression of *Arhgef1* in BMDMs (Fig. 5H). Additionally, the ChIP-qPCR assay demonstrated that the transcriptional regulation of FoxO1 led to the down-regulation of *Arhgef1* expression, as shown in Fig. 5I.

To investigate the potential involvement of ARHGEF1 in the migration of BMDMs, these cells were exposed to 10% FBS and fMLP. Migration induced by 10% FBS and fMLP was enhanced in the presence of Ad-FoxO1. However, this effect was suppressed when BMDMs were pre-treated with si-ARHGEF1, as shown in Fig. 5J. These findings suggest that FoxO1 plays a regulatory role in macrophage migration through its interaction with ARHGEF1.

3.6. FoxO1 inhibition decreased pro-inflammatory cytokines

ELISA analysis revealed lower levels of serum IL1β and IL6 proteins in myeloid FoxO1-deficient mice on Day 1 following renal I/R injury (Fig. 6A and B). Next, we employed Percoll gradients to isolate renal immune cells on Day 1 after I/R injury and assessed the mRNA expression of pro-inflammatory macrophage-associated genes. The real-time PCR analysis demonstrated a significant reduction in the expression of pro-inflammatory cytokines in response to I/R injury in mice with myeloid FoxO1 deficiency (Fig. 6C). Heat shock proteins (HSPs) are upregulated in response to inflammation to protect *in vitro* and *in vivo* cells from the toxic effects of inflammation-associated mediators[39]. Among the HSP family, HSP70 and HSP90 tightly regulate nuclear factor-κB signaling, a critical pathway in mediating inflammatory responses[40,41]. Our results showed that I/R-induced AKI increased the protein levels of HSP70 and HSP90 in the kidney, and myeloid FoxO1 deficiency inhibited this upregulation induced by I/R injury (Fig. 6D). Additionally, the effect of FoxO1 inhibition on LPS-induced inflammatory AKI was explored. As shown in Supporting Information Fig. S5A, our results showed that LPS didn't affect the levels of serum creatinine. However, LPS increased the levels of BUN compared with the sham group, and myeloid FoxO1 deficiency inhibited the LPS-induced increase (Fig. S5B). Moreover, myeloid FoxO1 deficiency inhibited increased mRNA expression of *Kim1* and *Ngal* induced by LPS (Fig. S5C). These results indicated that FoxO1 inhibition decreased inflammatory response to protect against AKI.

Furthermore, BMDMs isolated from mice with myeloid FoxO1 deficiency were treated with LPS and IFNγ. ELISA analysis of the culture supernatant revealed lower levels of IL1β protein, while there was no significant difference in IL6 protein levels (Fig. 6E and F). Similarly, the mRNA expression of pro-inflammatory macrophage-associated genes in BMDMs was reduced under LPS and IFNγ treatment when FoxO1 deficiency was present in the myeloid cells (Fig. 6G). In order to investigate the role of pro-inflammatory cytokines derived from macrophages in regulating tubular cell death, BMDMs were exposed to LPS and IFNγ for 24 h, after which the culture medium was replaced with a serum-free medium. Twelve hours later, the conditioned media (CM) from BMDMs was collected to treat mouse RTECs (Fig. 6H). The results obtained from TUNEL staining demonstrated a significant increase in mRTEC death when exposed to the CM derived from LPS and IFNγ-treated BMDMs. Conversely, a lower incidence of cell death was observed in mRTECs treated with CM from BMDMs with myeloid FoxO1 deficiency (Fig. 6I). This finding suggests that inhibiting FoxO1 can potentially safeguard tubular epithelial cells from death by reducing the levels of pro-inflammatory cytokines released from macrophages.

4. Discussion

The present study provides the first evidence that the administration of AS-Lipo, mainly acting on macrophages, has a protective effect on kidney injury. Furthermore, the use of myeloid FoxO1 deficiency mice provides additional evidence supporting the vital role of FoxO1 in regulating macrophage function in the I/R-induced AKI mice model, thereby suggesting its potential as a therapeutic target for AKI.

Macrophages exhibit heterogeneity and possess the ability to adapt their phenotype in response to the specific microenvironment. It is used to classify macrophages into two different phenotypes: classically activated (M1) phenotype and alternatively activated (M2) phenotype[42,43]. However, the M1/M2 classification is considered to oversimplify the true complexity of macrophages[44,45]. Growing evidence points out that macrophages simultaneously express classical M1 and M2 markers after injury[46,47]. Therefore, in this study, we prefer to define these cells as pro-inflammatory and anti-inflammatory macrophages based on their functions *in vivo*. Previous studies have demonstrated that FoxO1 has the capacity to bind to the promoter region of IL1β, thereby enhancing the activity of this promoter[48]. In response to LPS stimulation, FoxO1 exhibits a propensity for *trans*-activating the IL1β gene, thereby promoting the production of IL1β in macrophages[23]. Furthermore, FoxO1 is capable of activating the transcription of the C/EBPβ gene by directly binding to its promoter in adipocytes. This, in turn, leads to an upregulation of pro-inflammatory genes such as CCL2 and IL6[49]. Similarly, Tanaka et al.[50] discovered that FoxO1 binds to a forkhead site within the promoter region of the human iNOS gene in intact chromatin derived from human aortic endothelial cells. This suggests that FoxO1 plays a direct role in facilitating the polarization of macrophages towards the pro-inflammatory phenotype in the presence

of BMDMs after 200 nmol/L AS1842856 treatment. (F) Predicted binding sites for FoxO1 and ARHGEF1 by JASPAR online database. (G) Representative Western blots and quantifications of ARHGEF1 protein levels in peritoneal macrophages ($n = 3-4$). (H) The mRNA expression levels of *Arhgef1* in BMDMs after 200 nmol/L AS1842856 treatment ($n = 5$). (I) The binding of FoxO1 to ARHGEF1 is analyzed by ChIP-qPCR in RAW264.7 cells after 200 nmol/L AS1842856 treatment ($n = 4$). (J) Chemotactic responses to 10% FBS and fMLP of BMDMs were determined by Transwell migration assay ($n = 6$). Data are represented as mean ± SEM. *$P < 0.05$, **$P < 0.01$.

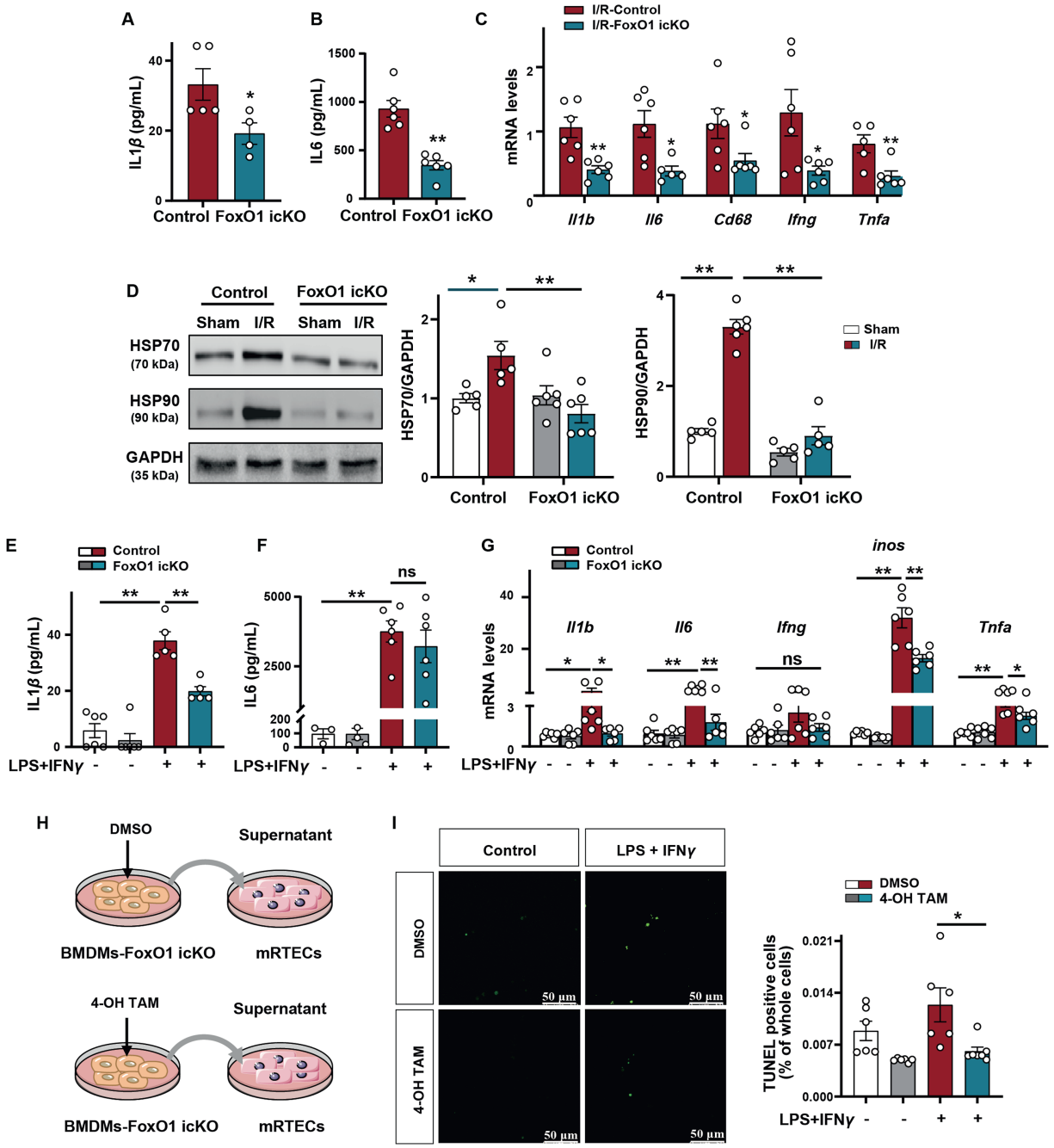

Figure 6 FoxO1 inhibition decreased pro-inflammatory cytokines. (A, B) ELISA indicated serum IL1β and IL6 protein levels of renal I/R injury mice on Day 1 (n = 4−6). (C) The mRNA expression levels of the inflammatory gene in renal myeloid cells on Day 1 after I/R injury (n = 5−6). (D) The protein levels of HSP70 and HSP90 in kidneys of renal I/R injury mice on Day 3 were detected by Western blotting (n = 5−6). (E, F) ELISA indicated IL1β and IL6 protein levels in the culture supernatant of BMDMs after treatment with LPS and IFNγ (n = 3−6). (G) The mRNA expression levels of the inflammatory gene in LPS and IFNγ treated BMDMs (n = 5−6). (H) Schematic diagram shows the treatment of BMDMs and mRTECs. (I) Representative images of TUNEL staining of mRTECs after treatment with culture supernatant of BMDMs, and quantitative analyses of TUNEL staining positive mRTECs (n = 6). Scale bar, 50 μm. Data are represented as mean ± SEM. $^*P < 0.05$, $^{**}P < 0.01$.

of inflammatory stimuli. Our findings also demonstrated that the inhibition of FoxO1 resulted in a reduction in the expression levels of genes associated with pro-inflammatory macrophages, such as *Il1b*, *Il6*, *iNos*, and *Tnfa*. Previous studies using animal models of AKI have indicated that there is a prevalence of a pro-inflammatory macrophage phenotype during the initial 1−3 days following injury[51]. Therefore, the decrease in pro-inflammatory macrophages caused by the inhibition of FoxO1 may contribute to the amelioration of kidney injury. Additionally, Luan and colleagues[52] reported that the number of renal pro-inflammatory macrophages

reached its peak on Day 14 and subsequently decreased by Day 30, whereas the number of anti-inflammatory macrophages progressively increased after Day 2 and peaked on Day 30 in a folic acid-induced AKI model. Zhou et al.[53] discovered that the presence of endothelial cells in a hypoxic environment, in combination with AS1842856, resulted in a decrease in the expression of the anti-inflammatory macrophage marker ARG1 in macrophages. Similarly, our study revealed that AS-Lipo treatment led to a reduction in the expression of anti-inflammatory macrophage-associated genes in BMDMs following IL4 stimulation. However, it is essential to note that our findings are based on a short-term *in vitro* model, and a comprehensive understanding of the role of FoxO1 in anti-inflammatory macrophage regulation necessitates a long-term *in vivo* model.

Following kidney injury, TECs generate inflammatory factors, including IL1β, IL18, IL15, IL16, and TNFα, which contribute to the inflammatory reaction[54]. Moreover, necrotic TECs secrete chemokines to attract macrophages to the site of injury[5,8]. This recruitment of macrophages is supported by previous studies, which discovered that exosomal *Ccl2* mRNA derived from TECs treated with BSA can be transported to interstitial macrophages, leading to their activation and autocrine recruitment of additional myeloid cells[55]. These infiltrating macrophages generate reactive oxygen species (ROS) and inflammatory cytokines like TNFα, which can intensify the apoptosis of tubular epithelial cells[56,57]. In our study, we observed a significant reduction in tubular epithelial cell death following treatment with conditioned media derived from myeloid FoxO1 deficiency BMDMs. These findings suggest that inhibiting FoxO1 can potentially protect against tubular epithelial cell death by decreasing the levels of pro-inflammatory cytokines released by macrophages. Moreover, our results showed that I/R-induced AKI increased the protein levels of HSP70 and HSP90, and myeloid FoxO1 deficiency inhibited this upregulation induced by I/R injury. These results suggested that FoxO1 inhibition suppressed macrophage-mediated inflammatory response and inhibited the inflammatory response involved in HSPs. Previous research has demonstrated that macrophages play a role in the repair processes of tubular epithelial cells by releasing cytokines like IL22 and providing ligands for retinoic acid and canonical Wnt-β catenin signaling[58]. However, further investigation is required to understand the full impact of FoxO1 on this repair mechanism.

NLRP3 inflammasome oligomerization results in the activation of caspase 1, then caspase 1 proteolytically cleaves pro-IL1β and pro-IL18 into their active forms, which target neighboring cells to propagate an inflammatory response[59,60]. A previous study found that mitochondrial damage during programmed cell death causes activation of the NLRP3 inflammasome[61]. Mitochondrial dysfunction acts upstream of NLRP3 activation by providing ROS to trigger NLRP3 oligomerization or by inducing α-tubulin acetylation to relocate mitochondria to the proximity of NLRP3[62]. Importantly, renal I/R injury induces NLRP3 inflammasome activation and an enhanced NLRP3 colocalization with mitochondria[63]. Our previous study found that FoxO1 inhibition significantly suppressed the overproduction of mitochondrial ROS (mtROS) in both I/R injury mice and hypoxia/reoxygenation human renal TECs[18]. Another study indicated that excessive mtROS impaired macrophage efferocytosis and reduced anti-inflammatory and pro-healing signals[64]. Therefore, the mechanism of decreased inflammatory response in the kidney after macrophage FoxO1 inhibition may be associated with suppressed mtROS production, which needs further experimental evidence.

FoxO1 is widely expressed in various renal parenchymal cells, such as podocytes, mesangial cells, and tubular epithelial cells[65]. Previous studies have demonstrated the involvement of FoxO1 in several kidney diseases, including AKI, diabetic kidney disease, and renal fibrosis[17,66-68]. It is important to note that the specific roles of FoxO1 in these diseases vary. Our previous studies have indicated that renal I/R injury leads to an up-regulation of FoxO1 expression in the kidney[18]. However, Zhang et al.[65] discovered that the downregulation of FoxO1 in mRTECs and the resulting mitochondrial damage contribute to the development of endotoxin-induced AKI. Conversely, the over-expression of FoxO1 through focal adeno-associated virus delivery to the kidney has been shown to enhance renal function and mitigate mitochondrial damage. Here, we provide evidence of a positive correlation between the expression of FoxO1 in the kidney and the severity of kidney trauma following AKI induced by I/R injury. Additionally, we have identified an upregulation of FoxO1 in renal macrophages subsequent to I/R injury. To demonstrate the impact of FoxO1 on macrophages in the context of I/R injury, we employed a FoxO1 inhibitor AS-Lipo that mainly acts on macrophages and observed its effective mitigation of renal damage caused by I/R injury. Similarly, using myeloid-specific FoxO1-knockout (Lyz2-Cre^{ERT2} *FoxO1*$^{flox/flox}$) mice also conferred protection against I/R-induced AKI. These contradictory findings may be attributed to variations in the AKI induction models employed, as well as the distinct cell types involved in the investigation. Specifically, the infiltration of macrophages into the kidney promotes the initiation of the inflammatory cascade within a mere 2 h of reperfusion[69]. Previous

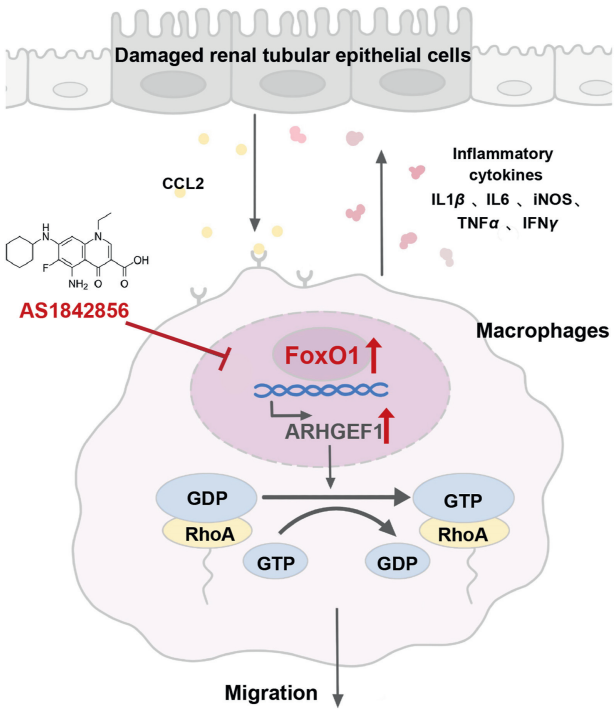

Figure 7 Renal I/R injury upregulated macrophage FoxO1 expression, inhibitors targeting macrophage FoxO1 could suppress macrophage infiltration and chemotaxis, as well as the inhibition of inflammatory factor-induced damage to mRTECs, thus alleviating I/R-induced AKI.

studies have indicated the presence of endotoxin tolerance in macrophages, with endotoxin-tolerant macrophages exhibiting similarities to anti-inflammatory macrophages[70]. Additionally, we observed an upregulation of FoxO1 expression and a decrease in FoxO3 expression in renal I/R injury. Interestingly, we found a negative correlation between FoxO3 and tubular necrosis, in contrast to FoxO1. This observation may be attributed to the complementary expression of *FoxO1*, *FoxO3*, and *FoxO4* mRNA in embryos[71]. A previous study has reported that FoxO1 and FoxO3 exhibit differential regulation of gene expression in HUVECs[72]. Consequently, further investigation is required to elucidate the interaction between FoxO1 and FoxO3 in I/R-induced AKI.

RhoA is a widely expressed cytoplasmic protein belonging to the small GTPase family, functioning as a molecular switch that regulates the activation of cytoskeletal proteins[73,74]. In their study, Rougerie et al.[75] discovered that Fam65b, a target of FoxO1, suppresses chemokine-induced migration by inhibiting RhoA activity, indicating a functional connection between FoxO1 and RhoA pathways. Similarly, our *in vitro* experiments with macrophages revealed that overexpression of FoxO1 significantly enhances RhoA activation. The expression of GTP-RhoA was observed to decrease upon FoxO1 inhibition. ARHGEF1, an intracellular protein expressed by hematopoietic cells, is known to activate RhoA and plays a crucial role in leukocyte migration and adhesion[37,38]. This activation occurs through RhoA GTPase[76]. Previous research has demonstrated that the absence of ARHGEF1 in neutrophils and B lymphocytes leads to impaired migration and adhesion[77]. In our study, we found that the expression of both ARHGEF1 and RhoA GTPase decreased in BMDMs following FoxO1 inhibition. Additionally, our study revealed that FoxO1 possesses a binding site on the promoter of ARHGEF1. Transwell experiments demonstrated that the overexpression of FoxO1 in BMDMs facilitated cell migration, but this effect was impeded upon knockdown of ARHGEF1. However, we observed that solely knocking down ARHGEF1 did not impact macrophage migration, potentially due to the inherent low migration of macrophages under normal conditions, such as without the overexpression of FoxO1. These findings suggest that ARHGEF1 serves as a potential mediator between FoxO1 and the activity of the RhoA pathway.

5. Conclusions

This study demonstrates that ablation of macrophage transcriptional factor FoxO1 protects against I/R-induced AKI. The primary mechanism underlying this effect involves the reduction in macrophage infiltration and chemotaxis, as well as the inhibition of inflammatory factor-induced damage to mice tubular epithelial cells (Fig. 7). In summary, FoxO1 is an important pathogenic mediator in AKI by regulating macrophage polarization, chemotaxis, and migration. AS-Lipo may represent a potential therapeutic strategy.

Acknowledgements

This work was supported by grants from the National Natural Science Foundation of China (No. 92168120 to Lu Tie), the Key Research and Development Project of Xinjiang Uygur Autonomous Region (2023B02010-5 to Lu Tie and Linlin Li, China), the Beijing Natural Science Foundation (No. Z200019 to Lu Tie, China), and grants from the National Natural Science Foundation of China (82073878, 81874318, 81473235 to Xuejun Li).

Author contributions

Yao He: Writing − review & editing, Writing − original draft, Methodology, Investigation, Conceptualization. Xue Yang: Writing − original draft, Methodology. Chenyu Zhang: Methodology, Formal analysis. Min Deng: Methodology, Data curation. Bin Tu: Project administration, Methodology. Qian Liu: Methodology. Jiaying Cai: Methodology. Ying Zhang: Methodology. Li Su: Methodology. Zhiwen Yang: Methodology. Hongfeng Xu: Methodology. Zhongyuan Zheng: Methodology. Qun Ma: Methodology. Xi Wang: Investigation. Xuejun Li: Funding acquisition, Conceptualization. Linlin Li: Supervision, Funding acquisition. Long Zhang: Writing-Reviewing and Editing. Yongzhuo Huang: Supervision, Conceptualization. Lu Tie: Writing − review & editing, Supervision, Investigation, Funding acquisition, Conceptualization.

Conflicts of interest

The authors declare no conflicts of interest.

Data availability statement

The data of RNA-seq supporting the findings of this study are openly available in repository Gene Expression Omnibus (GEO) at GSE250560.

Appendix A. Supporting information

Supporting information to this article can be found online at https://doi.org/10.1016/j.apsb.2025.04.009.

References

1. Federspiel CK, Itenov TS, Mehta K, Hsu RK, Bestle MH, Liu KD. Duration of acute kidney injury in critically ill patients. *Ann Intensive Care* 2018;**8**:30.
2. Xiao Z, Huang Q, Yang Y, Liu M, Chen Q, Huang J, et al. Emerging early diagnostic methods for acute kidney injury. *Theranostics* 2022; **12**:2963−86.
3. Coca SG, Singanamala S, Parikh CR. Chronic kidney disease after acute kidney injury: a systematic review and meta-analysis. *Kidney Int* 2012;**81**:442−8.
4. Hara M, Torisu K, Tomita K, Kawai Y, Tsuruya K, Nakano T, et al. Arginase 2 is a mediator of ischemia−reperfusion injury in the kidney through regulation of nitrosative stress. *Kidney Int* 2020;**98**:673−85.
5. Wang J, Xiong M, Fan Y, Liu C, Wang Q, Yang D, et al. Mecp2 protects kidney from ischemia−reperfusion injury through transcriptional repressing IL-6/STAT3 signaling. *Theranostics* 2022;**12**: 3896−910.
6. Deng LC, Alinejad T, Bellusci S, Zhang JS. Fibroblast growth factors in the management of acute kidney injury following ischemia−reperfusion. *Front Pharmacol* 2020;**11**:426.
7. Nakayama Y, Ueda S, Yamagishi S, Obara N, Taguchi K, Ando R, et al. Asymmetric dimethylarginine accumulates in the kidney during ischemia/reperfusion injury. *Kidney Int* 2014;**85**:570−8.
8. Jang HR, Rabb H. Immune cells in experimental acute kidney injury. *Nat Rev Nephrol* 2015;**11**:88−101.
9. Rudman-Melnick V, Adam M, Potter A, Chokshi SM, Ma Q, Drake KA, et al. Single-cell profiling of AKI in a murine model

reveals novel transcriptional signatures, profibrotic phenotype, and epithelial-to-stromal crosstalk. *J Am Soc Nephrol* 2020;**31**:2793−814.
10. Aslan A, van den Heuvel MC, Stegeman CA, Popa ER, Leliveld AM, Molema G, et al. Kidney histopathology in lethal human sepsis. *Crit Care* 2018;**22**:359.
11. Huen SC, Cantley LG. Macrophages in renal injury and repair. *Annu Rev Physiol* 2017;**79**:449−69.
12. Dong T, Chen X, Xu H, Song Y, Wang H, Gao Y, et al. Mitochondrial metabolism mediated macrophage polarization in chronic lung diseases. *Pharmacol Ther* 2022;**239**:108208.
13. Yao W, Chen Y, Li Z, Ji J, You A, Jin S, et al. Single cell RNA sequencing identifies a unique inflammatory macrophage subset as a druggable target for alleviating acute kidney injury. *Adv Sci (Weinh)* 2022;**9**:e2103675.
14. Pan Y, Cao S, Terker AS, Tang J, Sasaki K, Wang Y, et al. Myeloid cyclooxygenase-2/prostaglandin E2/E-type prostanoid receptor 4 promotes transcription factor MafB-dependent inflammatory resolution in acute kidney injury. *Kidney Int* 2022;**101**:79−91.
15. Orea-Soufi A, Paik J, Bragança J, Donlon TA, Willcox BJ, Link W. FOXO transcription factors as therapeutic targets in human diseases. *Trends Pharmacol Sci* 2022;**43**:1070−84.
16. Zhang J, Ng S, Wang J, Zhou J, Tan SH, Yang N, et al. Histone deacetylase inhibitors induce autophagy through FOXO1-dependent pathways. *Autophagy* 2015;**11**:629−42.
17. Xing YQ, Li A, Yang Y, Li XX, Zhang LN, Guo HC. The regulation of FOXO1 and its role in disease progression. *Life Sci* 2018;**193**:124−31.
18. Wang D, Wang Y, Zou X, Shi Y, Liu Q, Huyan T, et al. FOXO1 inhibition prevents renal ischemia−reperfusion injury *via* cAMP-response element binding protein/PPAR-γ coactivator-1α-mediated mitochondrial biogenesis. *Br J Pharmacol* 2020;**177**:432−48.
19. Wang YC, Ma HD, Yin XY, Wang YH, Liu QZ, Yang JB, et al. Forkhead Box O1 regulates macrophage polarization following *Staphylococcus aureus* infection: experimental murine data and review of the literature. *Clin Rev Allergy Immunol* 2016;**51**:353−69.
20. Lee S, Usman TO, Yamauchi J, Chhetri G, Wang X, Coudriet GM, et al. Myeloid FoxO1 depletion attenuates hepatic inflammation and prevents nonalcoholic steatohepatitis. *J Clin Investig* 2022;**132**: e154333.
21. Yang Y, Feng X, Liu X, Wang Y, Hu M, Cao Q, et al. Fate alteration of bone marrow-derived macrophages ameliorates kidney fibrosis in murine model of unilateral ureteral obstruction. *Nephrol Dial Transplant* 2019;**34**:1657−68.
22. Kawano Y, Nakae J, Watanabe N, Fujisaka S, Iskandar K, Sekioka R, et al. Loss of Pdk1−Foxo1 signaling in myeloid cells predisposes to adipose tissue inflammation and insulin resistance. *Diabetes* 2012;**61**: 1935−48.
23. Wang Y, Lyu Z, Qin Y, Wang X, Sun L, Zhang Y, et al. FOXO1 promotes tumor progression by increased M2 macrophage infiltration in esophageal squamous cell carcinoma. *Theranostics* 2020;**10**: 11535−48.
24. Paller MS, Neumann TV. Reactive oxygen species and rat renal epithelial cells during hypoxia and reoxygenation. *Kidney Int* 1991;**40**: 1041−9.
25. Chen B, Gao A, Tu B, Wang Y, Yu X, Wang Y, et al. Metabolic modulation *via* mTOR pathway and anti-angiogenesis remodels tumor microenvironment using PD-L1-targeting codelivery. *Biomaterials* 2020;**255**:120187.
26. Sasaki K, Terker AS, Pan Y, Li Z, Cao S, Wang Y, et al. Deletion of myeloid interferon regulatory factor 4 (Irf4) in mouse model protects against kidney fibrosis after ischemic injury by decreased macrophage recruitment and activation. *J Am Soc Nephrol* 2021;**32**:1037−52.
27. Jacobs FM, van der Heide LP, Wijchers PJ, Burbach JP, Hoekman MF, Smidt MP. FoxO6, a novel member of the FoxO class of transcription factors with distinct shuttling dynamics. *J Biol Chem* 2003;**278**: 35959−67.
28. Huang W, Wang BO, Hou YF, Fu Y, Cui SJ, Zhu JH, et al. JAML promotes acute kidney injury mainly through a macrophage-dependent mechanism. *JCI Insight* 2022;**7**:e158571.
29. Kelly C, Jefferies C, Cryan SA. Targeted liposomal drug delivery to monocytes and macrophages. *J Drug Deliv* 2011;**2011**:727241.
30. Li S, Zhang Y, Lu R, Lv X, Lei Q, Tang D, et al. Peroxiredoxin 1 aggravates acute kidney injury by promoting inflammation through Mincle/Syk/NF-κB signaling. *Kidney Int* 2023;**104**:305−23.
31. Kristianto J, Johnson MG, Zastrow RK, Radcliff AB, Blank RD. Spontaneous recombinase activity of Cre-ERT2 *in vivo*. *Transgenic Res* 2017;**26**:411−7.
32. Ilchuk LA, Stavskaya NI, Varlamova EA, Khamidullina AI, Tatarskiy VV, Mogila VA, et al. Limitations of tamoxifen application for *in vivo* genome editing using Cre/ERT2 System. *Int J Mol Sci* 2022;**23**:14077.
33. Kale J, Osterlund EJ, Andrews DW. BCL-2 family proteins: changing partners in the dance towards death. *Cell Death Differ* 2018;**25**: 65−80.
34. Wang Q, Zhang L, Yuan X, Ou Y, Zhu X, Cheng Z, et al. The relationship between the Bcl-2/Bax proteins and the mitochondria-mediated apoptosis pathway in the differentiation of adipose-derived stromal cells into neurons. *PLoS One* 2016;**11**:e0163327.
35. Mouton AJ, DeLeon-Pennell KY, Rivera Gonzalez OJ, Flynn ER, Freeman TC, Saucerman JJ, et al. Mapping macrophage polarization over the myocardial infarction time continuum. *Basic Res Cardiol* 2018;**113**:26.
36. Bisaria A, Hayer A, Garbett D, Cohen D, Meyer T. Membrane-proximal F-actin restricts local membrane protrusions and directs cell migration. *Science* 2020;**368**:1205−10.
37. Mathew D, Kremer KN, Torres RM. ARHGEF1 deficiency reveals Gα13-associated GPCRs are critical regulators of human lymphocyte function. *J Clin Investig* 2019;**129**:965−8.
38. Brown JP, Taube C, Miyahara N, Koya T, Pelanda R, Gelfand EW, et al. Arhgef1 is required by T cells for the development of airway hyperreactivity and inflammation. *Am J Respir Crit Care Med* 2007;**176**:10−9.
39. Ikwegbue PC, Masamba P, Mbatha LS, Oyinloye BE, Kappo AP. Interplay between heat shock proteins, inflammation and cancer: a potential cancer therapeutic target. *Am J Cancer Res* 2019;**9**:242−9.
40. Bai L, Xu S, Chen W, Li Z, Wang X, Tang H, et al. Blocking NF-κB and Akt by Hsp90 inhibition sensitizes Smac mimetic compound 3-induced extrinsic apoptosis pathway and results in synergistic cancer cell death. *Apoptosis* 2011;**16**:45−54.
41. Lyu Q, Wawrzyniuk M, Rutten VPMG, van Eden W, Sijts AJAM, Broere F. Hsp70 and NF-κB mediated control of innate inflammatory responses in a canine macrophage cell line. *Int J Mol Sci* 2020;**21**: 6464.
42. Chen T, Cao Q, Wang Y, Harris DCH. M2 macrophages in kidney disease: biology, therapies, and perspectives. *Kidney Int* 2019;**95**: 760−73.
43. Mantovani A, Sica A, Locati M. Macrophage polarization comes of age. *Immunity* 2005;**23**:344−6.
44. Blériot C, Chakarov S, Ginhoux F. Determinants of resident tissue macrophage identity and function. *Immunity* 2020;**52**:957−70.
45. Yan L, Wang J, Cai X, Liou YC, Shen HM, Hao J, et al. Macrophage plasticity: signaling pathways, tissue repair, and regeneration. *MedComm* 2024;**5**:e658.
46. Mesquida-Veny F, Del Río JA, Hervera A. Macrophagic and microglial complexity after neuronal injury. *Prog Neurobiol* 2021;**200**: 101970.
47. Pisu D, Huang L, Narang V, Theriault M, Lê-Bury G, Lee B, et al. Single cell analysis of *M. tuberculosis* phenotype and macrophage lineages in the infected lung. *J Exp Med* 2021;**218**:e20210615.
48. Su D, Coudriet GM, Hyun Kim D, Lu Y, Perdomo G, Qu S, et al. FoxO1 links insulin resistance to proinflammatory cytokine IL-1β production in macrophages. *Diabetes* 2009;**58**:2624−33.
49. Wang Y, Zhou Y, Graves DT. FOXO transcription factors: their clinical significance and regulation. *BioMed Res Int* 2014;**2014**:925350.
50. Tanaka J, Qiang L, Banks AS, Welch CL, Matsumoto M, Kitamura T, et al. Foxo1 links hyperglycemia to LDL oxidation and endothelial nitric oxide synthase dysfunction in vascular endothelial cells. *Diabetes* 2009;**58**:2344−54.

51. Gewin L, Zent R, Pozzi A. Progression of chronic kidney disease: too much cellular talk causes damage. *Kidney Int* 2017;**91**:552−60.
52. Luan J, Fu J, Jiao C, Hao X, Feng Z, Zhu L, et al. IL-18 deficiency ameliorates the progression from AKI to CKD. *Cell Death Dis* 2022; **13**:957.
53. Zhou Y, Zeng J, Tu Y, Li L, Du S, Zhu L, et al. CSF1/CSF1R-mediated crosstalk between choroidal vascular endothelial cells and macrophages promotes choroidal neovascularization. *Investig Ophthalmol Vis Sci* 2021;**62**:37.
54. Li ZL, Lv LL, Tang TT, Wang B, Feng Y, Zhou LT, et al. HIF-1α inducing exosomal microRNA-23a expression mediates the cross-talk between tubular epithelial cells and macrophages in tubulointerstitial inflammation. *Kidney Int* 2019;**95**:388−404.
55. Lv LL, Feng Y, Wen Y, Wu WJ, Ni HF, Li ZL, et al. Exosomal CCL2 from tubular epithelial cells is critical for albumin-induced tubulointerstitial inflammation. *J Am Soc Nephrol* 2018;**29**:919−35.
56. Zhao H, Alam A, Soo AP, George AJT, Ma D. Ischemia−reperfusion injury reduces long term renal graft survival: mechanism and beyond. *EBioMedicine* 2018;**28**:31−42.
57. Chevalier RL, Forbes MS, Thornhill BA. Ureteral obstruction as a model of renal interstitial fibrosis and obstructive nephropathy. *Kidney Int* 2009;**75**:1145−52.
58. Kumar S. Cellular and molecular pathways of renal repair after acute kidney injury. *Kidney Int* 2018;**93**:27−40.
59. Krishnan SM, Ling YH, Huuskes BM, Ferens DM, Saini N, Chan CT, et al. Pharmacological inhibition of the NLRP3 inflammasome reduces blood pressure, renal damage, and dysfunction in salt-sensitive hypertension. *Cardiovasc Res* 2019;**115**:776−87.
60. Xu H, Chen J, Chen P, Li W, Shao J, Hong S, et al. Costunolide covalently targets NACHT domain of NLRP3 to inhibit inflammasome activation and alleviate NLRP3-driven inflammatory diseases. *Acta Pharm Sin B* 2023;**13**:678−93.
61. Shimada K, Crother TR, Karlin J, Dagvadorj J, Chiba N, Chen S, et al. Oxidized mitochondrial DNA activates the NLRP3 inflammasome during apoptosis. *Immunity* 2012;**36**:401−14.
62. Yu JW, Lee MS. Mitochondria and the NLRP3 inflammasome: physiological and pathological relevance. *Arch Pharm Res (Seoul)* 2016;**39**:1503−18.
63. Ni H, Ou Z, Wang Y, Liu Y, Sun K, Zhang J, et al. XBP1 modulates endoplasmic reticulum and mitochondria crosstalk *via* regulating NLRP3 in renal ischemia/reperfusion injury. *Cell Death Discov* 2023; **9**:69.
64. Cai S, Zhao M, Zhou B, Yoshii A, Bugg D, Villet O, et al. Mitochondrial dysfunction in macrophages promotes inflammation and suppresses repair after myocardial infarction. *J Clin Investig* 2023; **133**:e159498.
65. Zhang M, Dong W, Li Z, Xiao Z, Xie Z, Ye Z, et al. Effect of forkhead box O1 in renal tubular epithelial cells on endotoxin-induced acute kidney injury. *Am J Physiol Ren Physiol* 2021;**320**:F262−72.
66. Huang F, Wang Q, Guo F, Zhao Y, Ji L, An T, et al. FoxO1-mediated inhibition of STAT1 alleviates tubulointerstitial fibrosis and tubule apoptosis in diabetic kidney disease. *EBioMedicine* 2019;**48**:491−504.
67. Li Y, Liu P, Zhou Y, Maekawa H, Silva JB, Ansari MJ, et al. Activation of angiopoietin−Tie2 signaling protects the kidney from ischemic injury by modulation of endothelial-specific pathways. *J Am Soc Nephrol* 2023;**34**:969−87.
68. Zhang A, Li M, Wang B, Klein JD, Price SR, Wang XH. miRNA-23a/27a attenuates muscle atrophy and renal fibrosis through muscle−kidney crosstalk. *J Cachexia Sarcopenia Muscle* 2018;**9**:755−70.
69. Zhou L, Tang S, Li F, Wu Y, Li S, Cui L, et al. Ceria nanoparticles prophylactic used for renal ischemia-reperfusion injury treatment by attenuating oxidative stress and inflammatory response. *Biomaterials* 2022;**287**:121686.
70. Collins PE, Carmody RJ. The regulation of endotoxin tolerance and its impact on macrophage activation. *Crit Rev Immunol* 2015;**35**: 293−323.
71. Matsukawa M, Sakamoto H, Kawasuji M, Furuyama T, Ogawa M. Different roles of Foxo1 and Foxo3 in the control of endothelial cell morphology. *Genes Cells* 2009;**14**:1167−81.
72. Potente M, Urbich C, Sasaki K, Hofmann WK, Heeschen C, Aicher A, et al. Involvement of Foxo transcription factors in angiogenesis and postnatal neovascularization. *J Clin Investig* 2005;**115**:2382−92.
73. Bros M, Haas K, Moll L, Grabbe S. RhoA as a key regulator of innate and adaptive immunity. *Cells* 2019;**8**:733.
74. Li Y, Zhu T, Yang J, Zhang Q, Xu S, Ge S, et al. EHMT2 promotes tumorigenesis in GNAQ/11-mutant uveal melanoma *via* ARHGAP29-mediated RhoA pathway. *Acta Pharm Sin B* 2024;**14**:1187−203.
75. Rougerie P, Largeteau Q, Megrelis L, Carrette F, Lejeune T, Toffali L, et al. Fam65b is a new transcriptional target of FOXO1 that regulates RhoA signaling for T lymphocyte migration. *J Immunol* 2013;**190**: 748−55.
76. Rubtsov A, Strauch P, Digiacomo A, Hu J, Pelanda R, Torres RM. Lsc regulates marginal-zone B cell migration and adhesion and is required for the IgM T-dependent antibody response. *Immunity* 2005;**23**: 527−38.
77. Francis SA, Shen X, Young JB, Kaul P, Lerner DJ. Rho GEF Lsc is required for normal polarization, migration, and adhesion of formyl-peptide-stimulated neutrophils. *Blood* 2006;**107**:1627−35.